INSTITUTE FOR FUSION STUDIES

DOE/ET-53088-514 IFSR #514

Form Invariance in Convective-Diffusive Systems with Applications to Impurity Transport

S.M. MAHAJAN
Institute for Fusion Studies
The University of Texas at Austin
Austin, Texas 78712
and
P.M. VALANJU and W.L. ROWAN
Fusion Research Center
The University of Texas at Austin
Austin, Texas 78712

August 1991

THE UNIVERSITY OF TEXAS

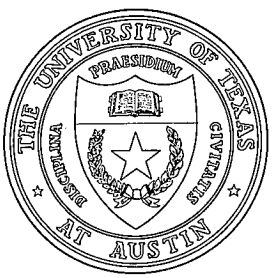

AUSTIN

Form Invariance in Convective-Diffusive Systems with Applications to Impurity Transport

S. M. Mahajan

Institute for Fusion Studies

P. M. Valanju and William L. Rowan

Fusion Research Center

The University of Texas at Austin

Austin, Texas 78712

Simple, closed form Green's functions are derived for convective-diffusive systems in slab and cylindrical geometries. In slab geometry, they are Gaussian, while in cylindrical geometry, they are of the form $e^{-\alpha r^2} I_o(\beta r)$, where I_o is the modified Bessel function, and α and β depend on time via e^{-t}. Time dependent profiles resulting from various pulsed and oscillatory sources can be obtained using these Green's functions. These solutions can be used to model a variety of time dependent transport experiments such as pulsed impurity transport, oscillating gas puff, perturbative RF heating, and sawtooth heat pulse propagation. A successful comparison of our profiles with pulsed impurity injection experiments on TEXT is presented.

1. Introduction

Perturbative experiments have become important tools in studying transport of particles, energy, and impurities in tokamaks. In these experiments, a variety of time dependent perturbations are used. These include impurity pulses, oscillating gas puff, modulated radio-frequency heating, and sawtooth heat pulses. If the perturbation is sufficiently small, one can make the linear assumption that the pulse responds to the ambient plasma without changing it. A simple phenomenological description of the process can then be given in terms of an effective diffusion coefficient D and inward convective speed V, which one can separately measure by observing the time evolution of the induced perturbation. In cylindrical geometry, such a system can be modeled by the linear, driven convective-diffusive equation

$$\mathcal{L}(F) \equiv \frac{\partial F(r,t)}{\partial t} + \frac{1}{r}\frac{\partial}{\partial r} r\Gamma(r,t) = s(r,t), \tag{1}$$

$$\Gamma(r,t) = -D\frac{\partial F}{\partial r} - rVF, \tag{2}$$

where $s(r,t)$ is the external source, Γ is the flux, D is the diffusion coefficient, rV is the convection speed, and F is the time dependent perturbed quantity (density, temperature, impurity density etc.). The linearity of Eq.(1) allows D and V to depend on r, but not directly on F.

The usual approach[1,2] taken in analysing the two dimensional (r and t dependent) experimental data with this model is to guess a form for D and V, solve the model numerically, and iterate the process until a good fit is obtained. It is, of course, expected that general analytical solutions of this system would be quite valuable in understanding broad features of the data, and in rapidly extracting the transport coefficients from it. Such solutions were available only in slab geometry with constant D and V. In a cylinder, a class of solutions was obtained[3] by setting the perturbed quantity to zero at the wall for all times. Such a condition is clearly

too restrictive : During the initial rise phase of an externally induced impurity pulse, and at all times during an oscillating gas puff, these solutions cannot be used.

In this paper, we calculate the Green's function for Eq.(1), and find that it has the simple form $e^{-\alpha r^2} I_o(\beta r)$, where I_o is the modified Bessel function, and α and β depend on time via e^{-t}. This function exhibits the same form-invariance as the Gaussian solution in slab geometry, viz., it maintains its functional identity as it evolves in time. Also, a sharp (delta function) initial pulse evolves into this shape. Using this Green's function, we obtain exact solutions for a variety of external sources. Due to the absence of any restrictive boundary conditions, these can be used to model any of the experiments described above. As an example, we present comparison of our results with pulsed impurity injection experiments[4] on TEXT.

2. Solutions in Slab Geometry

We start with a brief restatement of known results in slab geometry with constant D and V, where

$$\mathcal{M}(F) \equiv \frac{\partial F}{\partial t} - D\frac{\partial^2 F}{\partial x^2} - V\frac{\partial (xF)}{\partial x} = s(x,t), \tag{3}$$

is to be solved for F. By rescaling x and t to the dimensionless variables $y^2 = x^2 V/D$, and $\tau = Vt$, we get

$$M(F) \equiv \frac{\partial F}{\partial \tau} - \frac{\partial^2 F}{\partial y^2} - \frac{\partial (yF)}{\partial y} = S(y,\tau). \tag{4}$$

The Green' function of this equation, i.e., the solution of $M(G) = \delta(y-y_0)\delta(\tau-\tau_0)$, is the displaced Gaussian in y,

$$G(y, y_0, \tau, \tau_0) = \frac{1}{\sqrt{2\pi(1-e^{-2(\tau-\tau_0)})}} \exp\left(-\frac{(y - y_0 e^{-(\tau-\tau_0)})^2}{2(1-e^{-2(\tau-\tau_0)})}\right). \tag{5}$$

In order to satisfy causality, we set $G(y, y_0; \tau, \tau_0) = 0$ for $\tau < \tau_0$. The response to an arbitrary external driving source $S(y,\tau)$ is obtained from this Green's function

by

$$F(y,\tau) = \int_{-\infty}^{\infty} d\rho d\eta G(y,\rho;\tau,\eta) S(\rho,\eta). \tag{6}$$

This leads to a Gaussian response for a Gaussian driving source.

The sourceless form of this equation admits a steady state profile of the form $F = F_0 \exp(-y^2/2)$ due to the balance between diffusion and convection. Also, a sharp initial pulse $F(y, \tau = 0) = A\delta(y - y_0)$ evolves into the Gaussian shape $G(y, y_0; \tau, 0)$, leading to the asymptotic steady state

$$\tau \to \infty, \; F \to \frac{\mu}{\sqrt{2\pi}} \exp(\frac{-y^2}{2}). \tag{7}$$

It is also well known that an initial Gaussian pulse in space stays Gaussian as it propagates and spreads.

3. Solutions in Cylindrical Geometry

We now derive similar results in cylindrical geometry with the basic model given by Eq.(1). Upon rescaling to dimensionless variables $y = r^2V/2D$, and $\tau = 2Vt$, it is transformed into

$$L(F) \equiv \frac{\partial F}{\partial \tau} - \frac{\partial}{\partial y} y \frac{\partial F}{\partial y} - \frac{\partial (yF)}{\partial y} = S(y,\tau). \tag{8}$$

The Green's function $G(y, y_0, \tau, \tau_0)$ for the operator L satisfies

$$L(G) = \delta(\tau - \tau_0)\delta(y - y_0), \tag{9}$$

with dimensionless $y_0 = a^2V/2D$, where a is the radial location of the source. Expanding G in terms of Laguerre polynomials

$$G(y, y_0; \tau, \tau_0) = e^{-y} \sum_{n=0}^{\infty} a_n(\tau, \tau_0, y_0) L_n(y), \tag{10}$$

and using the orthogonality relation

$$\int_0^\infty dy L_n(y) L_m(y) e^{-y} = \delta_{m,n}, \tag{11}$$

we obtain, for each coefficient,

$$\frac{da_n}{d\tau} + n a_n = \delta(\tau - \tau_0) L_n(y_0). \tag{12}$$

Integrating this equation, and setting $a_n = 0$ for $\tau < \tau_0$, gives

$$G(y, y_0; \tau, \tau_0) = e^{-y} \sum_{n=0}^{\infty} e^{-n(\tau - \tau_0)} L_n(y_0) L_n(y). \tag{13}$$

Using the formula for the infinite sum,

$$\sum_{n=0}^{\infty} L_n(x) L_n(y) z^n = \frac{1}{1-z} \exp\left(-\frac{z(x+y)}{1-z}\right) I_0\left(\frac{2\sqrt{xyz}}{1-z}\right), \tag{14}$$

one obtains the simple, concise form for the causal Green's function

$$G(y, y_0; \tau, \tau_0) = X \exp\left(-X(y + y_0 x)\right) I_0\left(2X\sqrt{y y_0 x}\right) \theta(\tau - \tau_0), \tag{15}$$

where $\theta(x)$ is the Heaviside function [$\theta(x) = 0$ for $x < 0$, and $\theta(x) = 1$ for $x \geq 0$],

$$X = \frac{1}{1-x}, \tag{16}$$

$$x = \exp(-(\tau - \tau_0)). \tag{17}$$

The solution for an arbitrary source $S(y, \tau)$ can now be written in terms of this Green's function as

$$F(y, \tau) = \int_{-\infty}^{\infty} d\eta \int_0^\infty d\rho G(y, \rho; \tau, \eta) S(\rho, \eta), \tag{18}$$

where we have used the causality of G to extend the upper limit of the time integral from τ to ∞.

The Green's function of Eq.(15) is the analogue of the Gaussian in slab. Just as an initial Gaussian pulse evolving via the Cartesian Eq.(4) remains a Gaussian for all times, an initial pulse of the form in Eq.(15), i.e.,

$$S(y,\tau) = \delta(\tau)e^{-\alpha(y+y_0)}I_0(2\alpha\sqrt{yy_0}), \tag{19}$$

governed by Eq.(8) also maintains its form : The explicit solution is the form-invariant expression

$$F(y,\tau) = \frac{1}{\alpha(1-\chi)+\chi}\exp\left(-\frac{\alpha(y+\chi y_0)}{\alpha(1-\chi)+\chi}\right)I_0\left(\frac{2\alpha\sqrt{yy_0\chi}}{\alpha(1-\chi)+\chi}\right), \tag{20}$$

where $\chi = e^{-\tau}$. The sourceless form of this equation also admits a steady state solution of the same form. Finally, a delta function initial pulse evolves into this same shape, and approaches a nonzero asymptotic steady state.

In pulsed impurity injection experiments, the initial external source can be assumed to be a delta function. The solution is then just the single-term Green's function of Eq.(15). The more general choice (19) of the external source allows considerable flexibility in modeling other experimental situations. It can be made to peak near the edge (or the center) by choosing a large (or small) value of α. It can also be used in experiments where the external source is oscillatory. By fourier analyzing the time dependent part

$$S(y,\tau) = e^{-\alpha y}I_0(2\alpha\sqrt{y})\sum a_n sin(n\omega\tau), \tag{21}$$

and carrying out the space integral, we get, for each sinusoidal component

$$T_n = \int_{e^{-\tau}}^{1} dz \frac{z^{in\omega}}{2z(\alpha(1-z)+z)} \exp\left(-\frac{\alpha(y-\alpha(1-z))}{\alpha(1-z)+z}\right)I_0\left(\frac{2\alpha\sqrt{zy}}{\alpha(1-z)+z}\right). \tag{22}$$

This equation can be used to directly calculate the phase and the amplitude of the oscillating quantity as a function of r for each fourier component.

4. Long time decay of the pulse

This model requires an additional feature, edge loss, so that it can realistically model pulsed impurity injection experiments. The injected impurities disappear from the plasma after some interval because impurity ions which diffuse across the plasma boundary are not recycled. The solution described in the previous section does not include any loss mechanism: it relaxes to a nonzero steady state at large times due to the balancing effects of D and V. We can model the impurity loss by adding a term proportional to the perturbation F at the plasma edge ($y = \lambda$). For the case of the initial delta function source, the resulting pulse is the solution of

$$L(F) = \delta(\tau)\delta(y-\rho) - A\delta(y-\lambda)F(y,\tau), \tag{23}$$

where A has dimensions of velocity. Although in specific cases (such as impurity transport) A can be related to D, V, and the mean free path, in general it is treated here as a free parameter. Equation (23) is readily transformed into an integral equation by using the Green's function solution of Eq.(18). We perform the spatial integral to obtain

$$F(y,\tau) = G(y,\rho,\tau,0) - A\int_0^\tau d\eta G(y,\lambda,\tau,\eta)F(\lambda,\eta), \tag{24}$$

where we have assumed the perturbation to be zero before $\tau = 0$. This equation can be solved easily by discretizing the time into n steps to turn the integral into a sum

$$F(y,\tau_i) = G(y,\rho,\tau_i,0) - A\Delta\tau\sum_{j=1}^{n} G(y,\lambda,\tau_i,\tau_j)F(\lambda,\tau_j). \tag{25}$$

We first invert the $n \times n$ matrix equation to obtain $F(\lambda,\tau_i)$ at the sink location, and then use it in the sum to obtain $F(y,\tau_i)$ at all other locations. The decay rate of the solution after the initial rise is controlled by the sink strength A. A similar procedure can be followed for arbitrary sources and sinks.

5. Comparison with impurity pulse experiments

We now demonstrate one practical use of our solutions by modeling data from Scandium (Sc) injection into the TEXT[4] tokamak. In these experiments, the Sc puff was initiated outside the plasma by laser ablation. The temporal evolution of radial profiles of chord-averaged emission from successive ionization stages of Sc was spectroscopically observed. The low ion charge states (Sc^{+7} to Sc^{+10}) radiate near the wall, where the perturbed profiles change quickly in response to the external pulse and sink. The higher charge states (Sc^{+12} to Sc^{+18}) radiate progressively deeper in the plasma, where the pulse reaches its peak later and decays slower. We expect from atomic physics, and also notice from the data, that only a few states are present at each radius, and that there are radii where just one state dominates. Therefore, the time evolution of each charge state at its own peak radius will be taken to represent the time evolution of the total impurity density which is described by our model. In comparing the data with the model, we look for a combination of D, V, and A that reproduces all observed traces.

The time evolution of full radial profiles was measured for three charge states (9, 12, and 18) of Scandium. They were found to peak at 27, 16, and 0 cm respectively. A comparison between experimental and predicted signals at their peak locations is shown in fig.1. Only the trace for Sc^{+18}, which peaks in the center, is used to set the coefficients at $D = 1.85 \pm 0.05$ m^2/s, $V = 10 \pm 10$ m/s, and $A = 7.5 \pm 0.5$ m/s. Using these values, we predict all the other traces. Clearly, all features of the data are well modeled by our profiles with constant D, V, and an edge sink.

Time evolution of chord averaged signals was also measured for charge states 7, 8, 10, 13, 15, 16, and 17. Since the spatial locations for these ions were not measured, we can only deduce the radii (27, 27, 22, 14, 13, 12, and 10 cm

respectively) where our results best match the data. Three of these are also shown in fig.1. For high charge states ($\geq$12), each trace amplitude is normalized to match the peak in the data with the peak in the calculation. The lower charge states ($\leq$ 10) peak very near the plasma edge where their initial rapid buildup is governed by a competition between transport and atomic processes. The atomic time scales for ionization and recombination in the edge change from 1 to 30 ms within 2 cm. For charge states below 10, this is slower than the time at which the high initial peak is predicted by our transport calculation. The buildup to the peak is therefore expected to be slower than the 1 ms that our model predicts for these states. However, the later decay is on much longer time scales, and can be compared with the experiment directly. Therefore, the traces for the lower charge states are normalized to match at the peak in the data, and their subsequent decay is observed. .

With only three free parameters, our model does a good job of deducing nine signals. All three stages of the observed time evolution, viz., the rapid initial buildup, the time at which the peak is reached for different ionization stages, and the subsequent decay with continuously slowing down decay rate are predicted well by our model. Unlike the eigenfuction models[3] we are not restricted to analysing only the decaying stage of the pulse. We correctly predict the radial and temporal dependence of the decay rate. As expected, the average decay rate is faster at the edge than in the center. For each trace, the decay rate after the peak is initially rapid, and decreases to a constant value. All this indicates that the essential physics in this case is well represented. Our model is also applicable to many other experiments, some of which are currently under investigation.

Acknowledgments

The authors wish to thank Dr. A. Thyagaraja for helpful discussions. This work was supported by DOE GRANT DEFG-05-88ER53266.

References

[1] F. A. Haas, and A. Thyagaraja, Physica Scripta. **40**, 484 491 (1989).

[2] J. C. Wiley, W. H. Miner, and D. W. Ross, Controlled Fusion Theory Conference, Nevada, April 1984

[3] F. H. Seguin, R. Petrasso , and E. S. Marmar, Phys. Rev. Lett. **51**, 455 (1983).

[4] W. K. Leung, W. L. Rowan, J. C. Wiley, R. V. Bravenec, K. W. Gentle, W. L. Hodge, D. M. Patterson, P. E. Phillips, T. R. Price , and B. Richards, Plas. Phys. and Con. Fus. **28**, 1753 (1986).

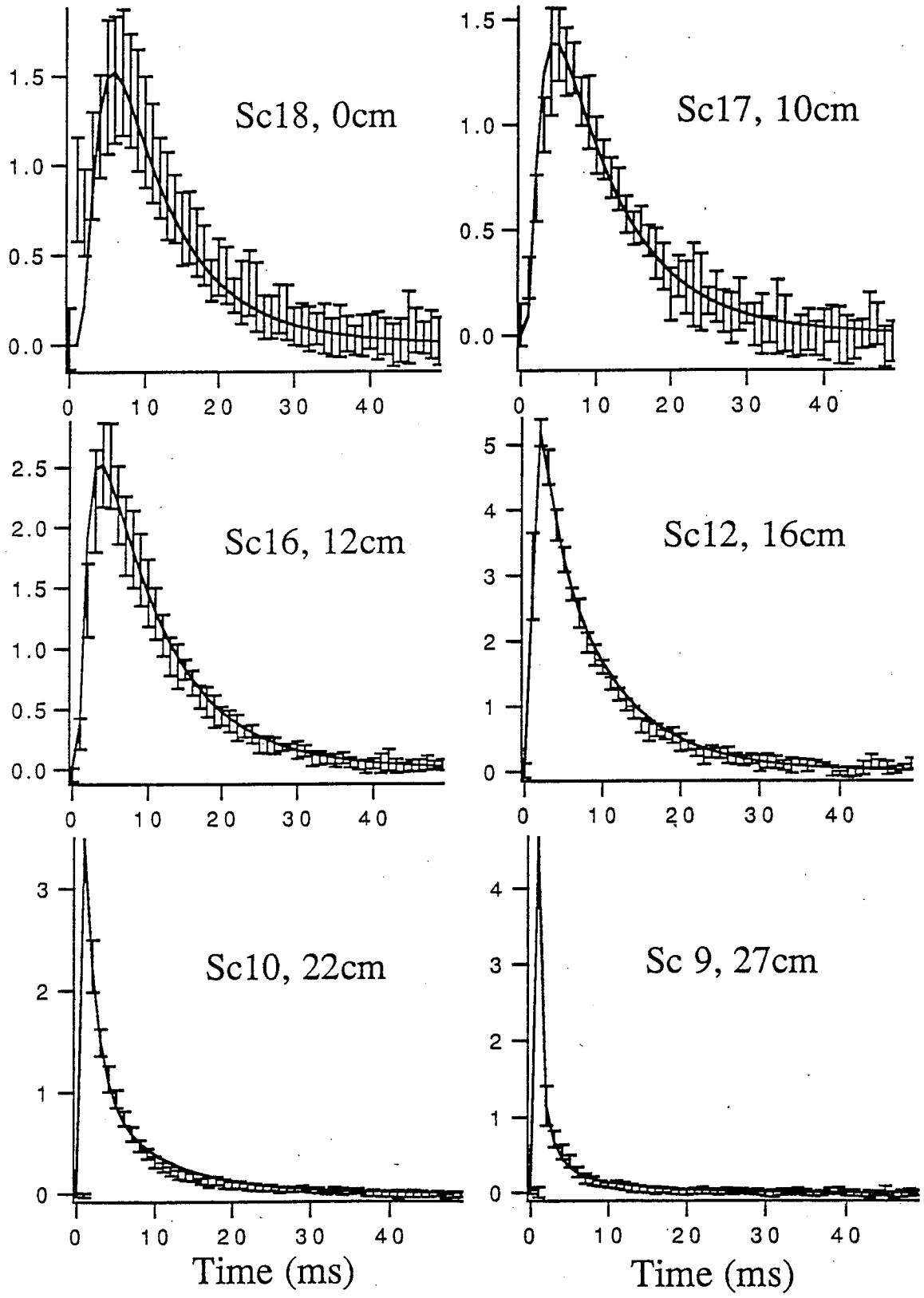

Fig. 1 Comparison between experimental measurements of time evolution of six Scandium lines and the predictions of our model for D=1.85 m^2/s, V=10 m/s, and A=7.5 m/s.